

**Band-structure-dependent nonlinear giant magnetoresistance in  $\text{Ni}_{1-x}\text{Fe}_x$  dual spin valves**N. Banerjee,<sup>1,\*</sup> J. W. A. Robinson,<sup>1</sup> A. Aziz,<sup>1</sup> M. Ali,<sup>2</sup> B. J. Hickey,<sup>2</sup> and M. G. Blamire<sup>1</sup><sup>1</sup>*Department of Materials Science and Metallurgy, University of Cambridge, Pembroke Street, Cambridge CB2 3QZ, United Kingdom*<sup>2</sup>*School of Physics and Astronomy, University of Leeds, Leeds LS2 9JT, United Kingdom*

(Received 24 September 2011; revised manuscript received 10 May 2012; published 24 October 2012)

Conventional giant magnetoresistance (GMR) in spin valves is current-independent, so the resistance of a device depends only on the relative orientation of the magnetic layers. In dual spin valves consisting of three ferromagnetic (FM) layers separated by nonmagnetic (NM) spacers (i.e., a FM1/NM/FM2/NM/FM1), GMR can be current-dependent if spin can accumulate in FM2 when outer FM1 layers are aligned antiparallel. Currently the underlying physics is poorly understood, although spin accumulation in FM2 is likely to depend on the gradient in the density of states at the Fermi energy of the ferromagnet. To investigate this hypothesis, we have measured a series of dual spin valves with  $\text{Ni}_{1-x}\text{Fe}_x$  as FM2 layers of varying composition. We show that both the magnitude and sign of the nonlinear GMR depend strongly on the Fe content and thus on the band structure of the ferromagnet FM2.

DOI: [10.1103/PhysRevB.86.134423](https://doi.org/10.1103/PhysRevB.86.134423)

PACS number(s): 85.75.-d, 72.25.Ba, 75.47.De, 85.70.Kh

**I. INTRODUCTION**

A difference in the density of states (DOS) at the Fermi energy ( $E_F$ ) for spin-up and spin-down electrons in a ferromagnet (FM) results in a spin polarization of a charge current passing through it. By extension, the conductivities of up- and down-spin electrons are different in a FM, and so the excess spins of the polarized current need to flip at the FM/NM interface in order to equalize the two spin channel populations in a nonmagnet (NM) which has equal conductivity for two spin channels. Under steady-state conditions, this gives rise to a spin accumulation at the FM/NM boundary, which decays into the bulk of the material with a characteristic length (the spin diffusion length). This spin accumulation is characterized by the splitting of the chemical potentials (Fermi energies) for up- and down-spin electrons near the FM/NM interface<sup>1,2</sup> and is an important concept for the analysis of current-perpendicular-to-plane giant magnetoresistance (CPP-GMR) in a FM/NM/FM spin valve (SV).<sup>3</sup> GMR can be understood by the differential scattering of spin-up and spin-down electrons in the bulk of the FMs and at FM/NM interfaces so that the total resistance depends on the relative orientation of the magnetization of the FM layers.<sup>4</sup> With the help of Boltzmann transport equations in a relaxation time approximation, the Valet-Fert (VF) theory<sup>3</sup> explains CPP-GMR by introducing phenomenological parameters of bulk ( $\beta$ ) and interfacial ( $\gamma$ ) scattering asymmetries defined as the fractional difference in the resistivities of the two spin channels associated with the FM bulk and the FM/NM interface, respectively. The scattering asymmetries are ultimately determined by the DOS for spin-up and spin-down electrons at  $E_F$ , and in standard VF theory the values are taken to be *independent* of current and hence independent of spin accumulation. This assumption implies that the spin-up and spin-down DOS are independent of energy near  $E_F$  and require GMR to be current-independent; this may be a reasonable approximation given the low absolute values of chemical potential splitting in most GMR experiments.

One possible way to increase the spin accumulation, proposed originally as a means of enhancing spin transfer torque switching (STT),<sup>5</sup> is to use a FM1/NM/FM2/NM/FM1 dual spin valve (DSV) structure with antiparallel outer FM1 layers. Previous experiments with such structures have

revealed a current dependence of the GMR for large current densities<sup>6,7</sup> which requires an extension of standard VF theory to explain. Baláz and Barnaš have shown<sup>8</sup> theoretically that the experimental results can be reproduced by adding a linear current dependence to the values of  $\beta$  and  $\gamma$  associated with the FM2 layer. As discussed above, this implies an energy dependence of the FM2 DOS near  $E_F$  instead of a flat distribution as required by the assumption of VF theory.

In a diffusive device, even at large current densities, the chemical potential shifts associated with spin accumulation are small compared with the FM exchange splitting and below the resolution of direct experimental probes of the band structure such as photoemission. As an alternative test of our understanding, we chose to vary the band structure of the FM2 layer by using different  $\text{Ni}_{1-x}\text{Fe}_x$  alloy compositions.

**II. EXPERIMENT**

DSV structures were sputter-deposited on unheated  $10 \times 5 \text{ mm}^2$  Si/SiO<sub>2</sub> substrates with an active layer sequence of Co<sub>90</sub>Fe<sub>10</sub> (6 nm) / Cu (4 nm) /  $\text{Ni}_{1-x}\text{Fe}_x$  (2 nm) / Cu (4 nm) / Co<sub>90</sub>Fe<sub>10</sub> (6 nm) / IrMn (10 nm) in a chamber with a base pressure better than  $5 \times 10^{-8}$  mbar. In this paper, the different samples corresponding to different  $\text{Ni}_{1-x}\text{Fe}_x$  compositions, such as  $x = 0.2$  (Ni<sub>0.8</sub>Fe<sub>0.2</sub>), will be referred to as DSV(80-20) and the alloy as Ni<sub>80</sub>Fe<sub>20</sub>. Although the top CoFe layer is exchange-biased via the IrMn pinning layer, the full MR loops did not show significant bias. Above and below the DSV structure, we deposited 200-nm-thick Cu electrodes. We also deposited a 5 nm layer of Ta at the bottom and at the top to prevent oxidation of the Cu contacts and to minimize ion-beam damage from subsequent processing steps. Using standard optical lithography and Ar-ion milling, a series of 4- $\mu\text{m}$ -wide tracks were processed, each connected to four large area contact pads for four terminal electrical measurements. By using a focused ion beam (FIB) microscope, nanopillar devices were fabricated in the tracks (as described elsewhere)<sup>7,9,10</sup> with an average dimension of  $250 \times 250 \text{ nm}^2$ . Devices were then transferred to a custom-built probe for electrical measurements. The current-voltage characteristics were measured using a lock-in amplifier technique with a frequency of 3.46 kHz and an alternating current amplitude

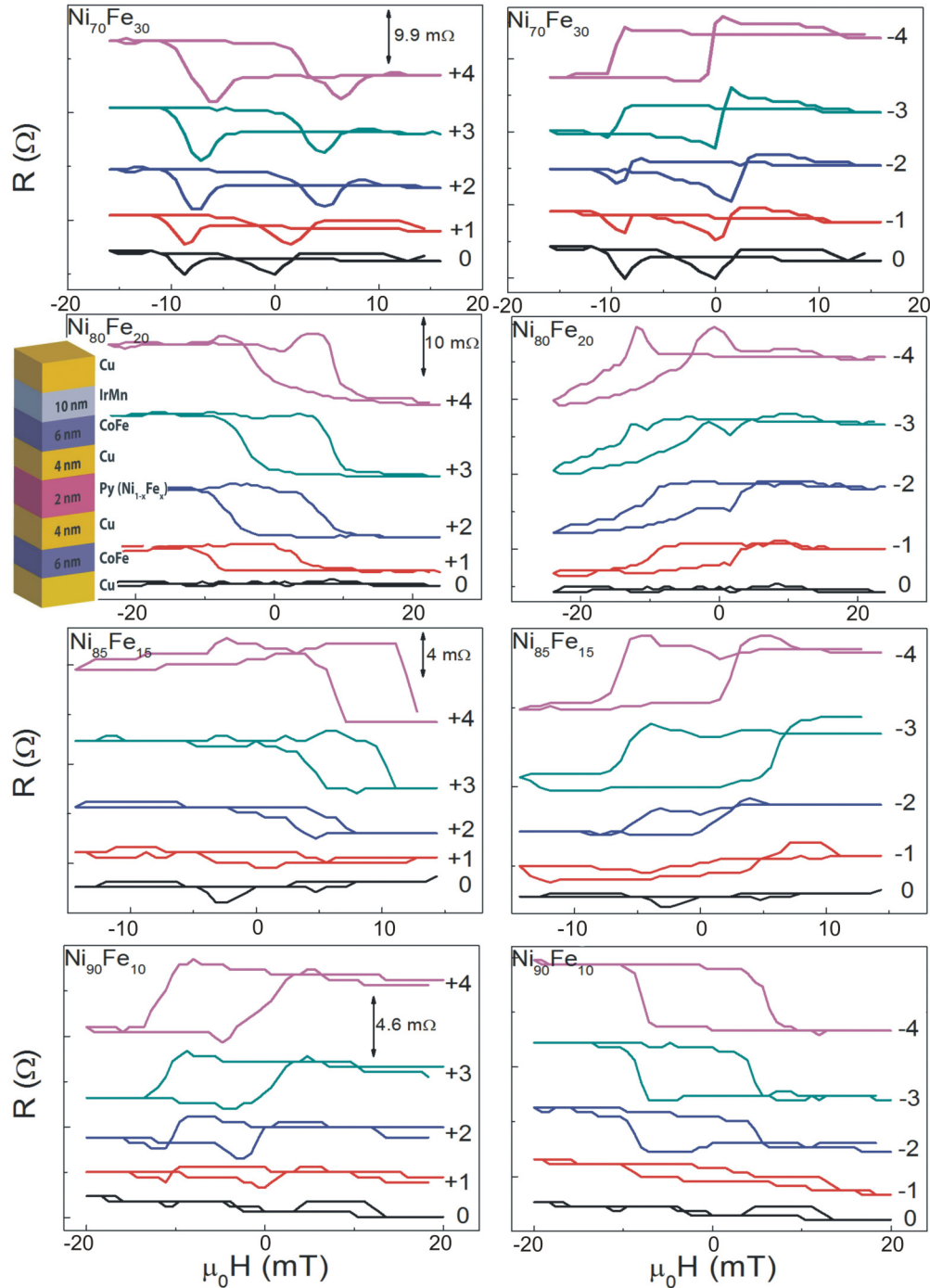


FIG. 1. (Color online) Minor loops as a function of applied bias current for DSVs with different FM2 layer compositions as indicated in each figure measured at room temperature. The numbers to the right of each graph show the magnitude of the dc bias current in mA. Positive current denotes electron flow from IrMn/CoFe to CoFe. The vertical bars in each figure denote the scale. The inset shows the layer sequence in the DSV stack.

of  $I_{ac} = 100 \mu A$  superimposed on a bias current ( $I_{dc}$ ) at room temperature. A positive value of  $I_{dc}$  corresponds to electrons flowing from the IrMn/CoFe layer to the lower CoFe layer.

### III. RESULTS

The DSV devices consist of three FM layers decoupled by Cu spacers, as shown in the inset of Fig. 1, which

makes it possible to obtain a variety of magnetic states by controlling the relative magnetization directions of the three FM layers. A detailed description of the magnetic states in a DSV is given in Ref. 7. The most relevant configurations for this study are the antiparallel (AP) states ( $\uparrow\uparrow\downarrow$  and  $\uparrow\downarrow\downarrow$ ) in which the magnetically soft FM2 layer is switched between opposite directions by a magnetic field which is too small to disturb the AP orientation of the outer layers. The

required switching behavior was confirmed by magnetization measurements on unpatterned 2-nm-thick films of the different  $\text{Ni}_{1-x}\text{Fe}_x$  compositions studied sandwiched between 200 nm Cu on  $\text{SiO}_2$  substrate.

For each  $\text{Ni}_{1-x}\text{Fe}_x$  composition, the differential resistance of the DSV devices as a function of magnetic field between the  $\uparrow\uparrow\downarrow$  and  $\uparrow\downarrow\downarrow$  states was recorded as a minor loop as a function of dc bias: examples are shown in Fig. 1. Standard VF theory would predict that the two resistance states  $\uparrow\uparrow\downarrow$  and  $\uparrow\downarrow\downarrow$  would be degenerate. It can be seen that, while this is true at zero bias, at finite current, reversing either the central magnetic layer or the current direction causes a resistance change, this difference becoming more pronounced with increasing current magnitude. This is the nonlinear giant magnetoresistance effect introduced previously,<sup>6-8</sup> and it is visible in DSV devices primarily because the conventional GMR effect is canceled by the AP orientation of the outer magnetic layers. Before we consider the implications of the results shown in Fig. 1, we will discuss the possible competing effects of Oersted fields generated by the currents through the device. In an earlier publication,<sup>6</sup> we used the fact that although there is a small effective field proportional to the applied current which can shift the forward and reverse switching fields by a small amount, the difference between the forward and reverse switching fields is essentially independent of current, which indicates that the switching takes place between the same magnetic states—and hence that these states are unaffected by current (see Figs. 1 and 2(b) in Ref. 6). To confirm this conclusion, we performed finite-element simulations using COMSOL MULTIPHYSICS 4.2a (Ref. 11) to estimate the Oersted field arising from the three-dimensional structure of the nanopillars. In Fig. 2, we show the result for a nanopillar with dimensions  $250 \times 250 \text{ nm}^2$ . For simplicity, we have assumed a 20-nm-thick permalloy layer sandwiched between 270 nm Cu electrodes [Fig. 2(a)] with a CPP geometry (current flow shown by black arrows) and surrounded by air. The Oersted field distribution over a cross section taken through the middle of the permalloy layer [Fig. 2(a)] for a current of 1 mA is shown in Fig. 2(b). The highest Oersted fields are at the middle of the four edges ( $\sim 1.5 \text{ mT}$ ), and the bulk of the layer experiences a field much lower than 1 mT. Due to minor nonuniformities in current flow at the boundaries of the nanopillar, the highest fields are not at the corners but at the edges. The maximum current-induced fields of 1.5 mT are confined to a very small region (a few nanometers) at the edges, and they are significantly lower than the switching fields that we observe for the minor loops ( $\sim 7\text{--}8 \text{ mT}$ ). By extension, this field is much smaller than fields required to destabilize the AP configuration of the outer magnetic layers. However, for a bias current of 4 mA, the Oersted field at the edges can be of the order of 5–6 mT. This field, coupled with the fringing fields generated by the outer CoFe layers, may lead to inhomogeneous magnetization configurations confined to a region of a few nanometers near the edges. These changes are too small to perturb the overall magnetic configuration and only minimally affect the associated resistance. The strongest proof in favor of the fact that the resistance changes do not originate from Oersted field effects comes from our previous<sup>6,7</sup> consistent observation of significant resistance modification between  $\uparrow\uparrow\downarrow$  and  $\uparrow\downarrow\downarrow$  states with a bias current of as low as

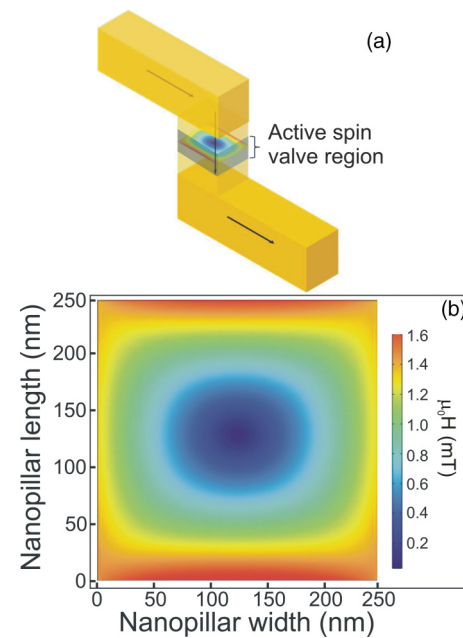


FIG. 2. (Color online) Finite-element simulation of the Oersted field in a nanopillar device with dimensions of  $250 \times 250 \text{ nm}^2$ . (a) The nanopillar geometry with the current flow direction indicated by black arrows. The Oersted field distribution is calculated at the middle of the nanopillar through a cross section as shown. (b) The field distribution for a current of 1 mA with the color scale denoting the magnitude of the magnetic field generated by the current in units of mT; the maximum field ( $\sim 1.5 \text{ mT}$ ) is at the middle of the edges of the pillar, and the bulk of the layer experiences a field of less than 1 mT.

$200 \mu\text{A}$  for devices with varying dimensions of up to 400 nm. The highest Oersted field in such devices for  $200 \mu\text{A}$  will be less than 0.1 mT, which is too low to induce any change in magnetic configuration even near the edges. The fact that the nonlinear behavior is independent of the device dimension and is present for such low bias currents conclusively rules out the role of the Oersted field as an underlying cause of the observed changes in Fig. 1 and confirms a more fundamental origin of the effect.

The change of resistance between  $\uparrow\uparrow\downarrow$  and  $\uparrow\downarrow\downarrow$  for  $\text{Ni}_{80}\text{Fe}_{20}$  has been reported previously,<sup>6,7</sup> but here we see similar changes even when the middle layer composition is changed, indicating the generality of this effect. DSV (70-30), DSV (80-20), and DSV (85-15) show similar trends of the variation of the sign of the resistance change with bias current which is reversed for DSV (90-10).

To make the resistance change ( $\Delta R$ ) independent of the device area, we look at the resistance-area product ( $A\Delta R$ ) as a function of dc bias current for different middle FM layer composition, as shown in Fig. 3. The DSV (70-30) and DSV(85-15) curves lie much below the DSV (80-20), while the DSV (90-10) is inverted with respect to the bias current direction, as is evident from the minor loops in Fig. 1. All compositions show a roughly linear region of  $A\Delta R$  at low bias and deviation from linearity at high bias values. A natural extension to this alloy series would be to study a DSV with pure Ni; however, despite fabricating many DSV devices with Ni as the FM2 layer, it was not possible to fully rotate the Ni layer while maintaining antiparallel FM1 layers.

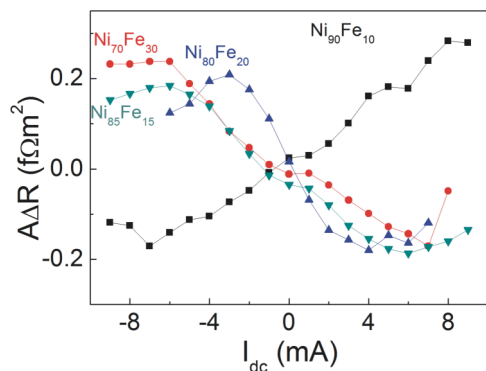


FIG. 3. (Color online) The change in the resistance-area product with current and middle  $\text{Ni}_{1-x}\text{Fe}_x$  layer composition. Each data point represents the average value of  $A\Delta R$  from many devices and chips measured.

#### IV. DISCUSSION

In our previous work,<sup>7</sup> we showed that for thicknesses of the FM2 layer close to its spin diffusion length, the magnitude of the nonlinear effect is determined by the bulk spin accumulation and subsequent modification of  $\beta$ . For smaller thicknesses (e.g., 2 nm used here), the interfacial spin accumulation, and hence current-dependent  $\gamma$ , has a more pronounced effect. We can make the comparison between the different alloys more quantitative by taking the gradient of  $A\Delta R$  in the linear portion of the data versus current density ( $J$ ) for each of the devices measured. In Fig. 4, we plot  $\alpha$  ( $=A\Delta R/J$ ), which represents the normalized magnitude of the nonlinear GMR, versus alloy composition, which shows a smooth variation as a function of Fe content. At the  $\text{Ni}_{1-x}\text{Fe}_x/\text{Cu}$  interface, poor matching of the spin-dependent atomic potentials for the minority spin band leads to strong minority electron scattering.<sup>12,13</sup> The interfacial scattering can be modeled by Mott scattering, where the scattering rate (and the resistance) for the minority spin channel is directly proportional to the corresponding DOS [ $g(E)$ ]. Thus we can write

$$\gamma \propto R_{\text{minority}} \propto g(E_F), \quad (1)$$

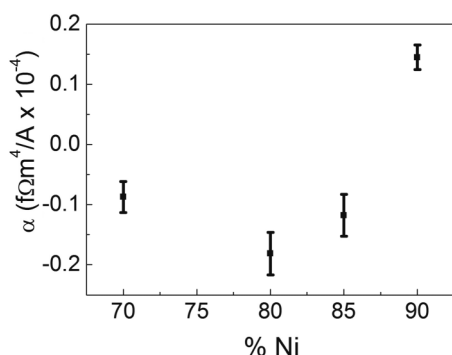


FIG. 4. Normalized magnitude of nonlinear GMR ( $\alpha$ ) defined by the slope of the linear region of resistance-area product ( $A\Delta R$ ) vs current density ( $J_{\text{dc}}$ ) as a function of Ni%. Each error bar represents one standard deviation measured from a set of  $A\Delta R$  vs  $J_{\text{dc}}$  data collected from several devices on different substrates.

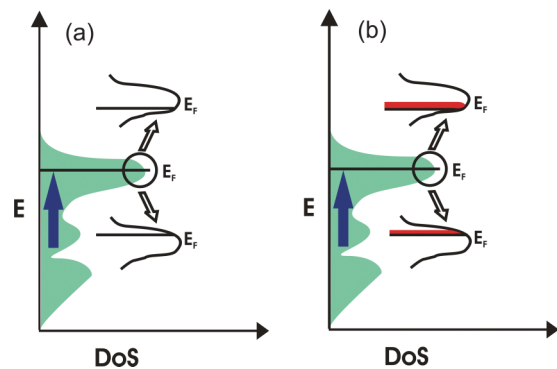


FIG. 5. (Color online) (a) Two possible locations of the Fermi energy with respect to the peak in density of states (DOS) without spin accumulation. (b) Spin accumulation on top of Fermi energy indicated by red bands. In the presence of a spin accumulation, electrons are transported through a different density of states (top of the red band).

where  $R_{\text{minority}}$  denotes the resistance of the minority spin channel.

Combining Eq. (1) with the definition of  $\alpha$ , we have

$$\alpha = \frac{d\gamma}{dJ} \propto \frac{dg(E)}{dJ} \propto \frac{dg(E)}{dE} \frac{dE}{dJ} \propto \frac{dg(E)}{dE} \frac{1}{g(E)}, \quad (2)$$

which relates  $\alpha$  with the DOS near the Fermi energy. It is clear from Fig. 3 that  $\text{Ni}_{80}\text{Fe}_{20}$  has a higher magnitude of  $\alpha$  compared to  $\text{Ni}_{70}\text{Fe}_{30}$  and  $\text{Ni}_{85}\text{Fe}_{15}$ , which from Eq. (2) implies a larger  $dg(E)/dE$  for  $\text{Ni}_{80}\text{Fe}_{20}$ . In an ideal flatband condition,  $dg(E) = 0$  and the resistances of  $\uparrow\uparrow\downarrow$  and  $\uparrow\downarrow\downarrow$  states are equal even under biased conditions giving rise to a zero  $\alpha$  value.

The most intriguing feature in Figs. 1 and 3 is the complete reversal of the current dependence for DSV (90-10), with  $A\Delta R$  being positive (instead of negative) for positive  $I_{\text{dc}}$ . This results in a positive  $\alpha$  as shown in Fig. 4. The fact that  $A\Delta R$  value remains independent of the device dimensions at a definite bias current and for a particular  $\text{Ni}_{1-x}\text{Fe}_x$  composition rules out any possible role of spin transfer torque induced perturbations as the underlying cause for a reversal of the sign of  $\alpha$ . A likely reason for this reversal can be attributed to the band structure of  $\text{Ni}_{1-x}\text{Fe}_x$  around the composition  $x = 0.1$ . Figure 5(a) shows two possible locations of  $E_F$  with respect to the peak in DOS without spin accumulation. In the presence of a spin accumulation [Fig. 5(b)] indicated by red bands, when  $E_F$  lies below the peak position, the electrons will be transported through an increasing DOS [i.e., a positive  $dg(E)/dE$ ] as it moves above the Fermi level with increasing bias current. On the other hand,  $E_F$  lying above the peak results in the electrons being transported through decreasing DOS with increasing spin accumulation. A reversal of  $dg(E)/dE$  reverses the sign of  $\alpha$  according to Eq. (2). This indicates the importance of the position of the Fermi energy in determining the sign of resistance change with bias current. The chemical potential shift associated with the spin accumulation is of the order of 0.1 meV (Ref. 8) in these systems. However, mapping of the band structure with such resolution is not currently possible using ARPES measurements or available computational techniques, so it is difficult to directly observe such a transition in the slope above  $E_F$  for  $\text{Ni}_{1-x}\text{Fe}_x$ .

alloys from band-structure measurements. Nonetheless, we can obtain some insights from the simulated band structure of  $\text{Ni}_{1-x}\text{Fe}_x$  alloys<sup>14</sup> at a lower energy resolution of 20 meV. Increasing Fe content changes the DOS near  $E_F$  for the minority spin subband, increasing minority electron scattering, while the majority spin subband is relatively unaffected. The variation in DOS around  $E_F$  gradually flattens out for Ni sites with increasing Fe content, which explains the reduced  $\alpha$  value for  $\text{Ni}_{70}\text{Fe}_{30}$  (Fig. 4) compared to  $\text{Ni}_{80}\text{Fe}_{20}$ .  $\text{Ni}_{80}\text{Fe}_{20}$  shows a strong suppression of the sharp minority spin band peak in Ni present in  $\text{Ni}_{90}\text{Fe}_{10}$ , which potentially explains the large change in  $\alpha$  value between these two compositions. Increasing Fe content beyond 20% does not show any abrupt change in DOS distribution as evident from the  $\text{Ni}_{50}\text{Fe}_{50}$  band structure, resulting in a relatively weaker dependence of  $\alpha$  on composition for this range.

The Fe sites in  $\text{Ni}_{90}\text{Fe}_{10}$  composition show a local decrease in DOS before the sharp peak just above  $E_F$  for the minority spin subband, which disappears for  $\text{Ni}_{80}\text{Fe}_{20}$  composition. Thus, the DOS above  $E_F$  indeed shows a reversal from a locally decreasing to a locally increasing trend between the composition range  $\text{Ni}_{90}\text{Fe}_{10}$  and  $\text{Ni}_{80}\text{Fe}_{20}$  supporting our explanation for the possible cause of reversal of sign of  $A\Delta R$  (and hence  $\alpha$ ) for  $\text{Ni}_{90}\text{Fe}_{10}$ .

Although significant spin accumulation is achieved in the  $\text{Ni}_{1-x}\text{Fe}_x$ -based DSV studied here, it is limited by the poor injection of spins across a FM/NM interface arising from the spin resistivity mismatch between  $\text{Ni}_{1-x}\text{Fe}_x$  and Cu and the low overall resistance of the device which limits the maximum current and voltage offset. To overcome this problem, a spin-selective resistive contact such as an insulating barrier (I) can be inserted between the FM and NM (i.e., FM/I/NM), which dramatically increases the spin accumulation and hence the spin injection efficiency. Recently, Fukuma *et al.* reported<sup>15</sup> giant enhancement of spin accumulation in NiFe/MgO/Ag lateral spin valves, where MgO reduces the

spin resistivity mismatch between NiFe and Ag. A DSV analog of such a device can be produced by incorporating two insulating barriers on both sides of the middle ferromagnet, i.e., the FM1/NM/I/FM2/I/NM/FM1 junction. Instead of using ferromagnetic outer layers, an alternative approach is to use spin filters (SFs) having different tunnel barrier heights for up- and down-spin electrons.<sup>16,17</sup> For outer antiparallel SF magnetizations, a very high spin accumulation can be generated in the middle ferromagnetic layer (FM) by using an active layer stack SF/I/FM2/I/SF connected to nonmagnetic contacts. In these systems, the nonlinear effect would scale proportionally to the spin accumulation, leading to much larger modification of the scattering asymmetry and hence larger resistance changes. Thus, by tuning the band structure in concomitance with the use of a tunnel barrier or SF, highly efficient full electronic control of the resistive state of a device can be achieved.

## V. CONCLUSION

In this article, we have shown the crucial role played by the band structure of the middle FM layer in a DSV in determining the magnitude and direction of the resistance change between  $\uparrow\uparrow\downarrow$  and  $\uparrow\downarrow\downarrow$  states under nonequilibrium conditions of spin accumulation. Importantly, this study establishes the link between band structure and current-induced modification of phenomenological parameters used in VF theory, thus providing an important understanding of scattering asymmetries in terms of band structure.

## ACKNOWLEDGMENTS

N.B. is supported by the Dr. Manmohan Singh Scholarship and J.W.A.R. by The Royal Society through a University Research Fellowship. This work was funded by the UK EPSRC through the Spin@RT consortium.

\*nb366@cam.ac.uk

<sup>1</sup>P. C. van Son, H. van Kempen, and P. Wyder, *Phys. Rev. Lett.* **58**, 2271 (1987).

<sup>2</sup>M. Johnson and R. H. Silsbee, *Phys. Rev. B* **37**, 5326 (1988).

<sup>3</sup>T. Valet and A. Fert, *Phys. Rev. B* **48**, 7099 (1993).

<sup>4</sup>M. N. Baibich, J. M. Broto, A. Fert, F. Nguyen Van Dau, F. Petroff, P. Etienne, G. Creuzet, A. Friederich, and J. Chazelas, *Phys. Rev. Lett.* **61**, 2472 (1988); G. Binasch, P. Grünberg, F. Saurenbach, and W. Zinn, *Phys. Rev. B* **39**, 4828 (1989).

<sup>5</sup>L. Berger, *J. Appl. Phys.* **93**, 7693 (2003).

<sup>6</sup>A. Aziz, O. P. Wessely, M. Ali, D. M. Edwards, C. H. Marrows, B. J. Hickey, and M. G. Blamire, *Phys. Rev. Lett.* **103**, 237203 (2009).

<sup>7</sup>N. Banerjee, A. Aziz, M. Ali, J. W. A. Robinson, B. J. Hickey, and M. G. Blamire, *Phys. Rev. B* **82**, 224402 (2010).

<sup>8</sup>P. Baláz and J. Barnaś, *Phys. Rev. B* **82**, 104430 (2010).

<sup>9</sup>C. Bell, G. Burnell, D.-J. Kang, R. H. Hadfield, M. J. Kappers, and M. G. Blamire, *Nanotechnology* **14**, 630 (2003).

<sup>10</sup>M. G. Blamire, A. Aziz, and J. W. A. Robinson, *Philos. Trans. R. Soc. A* **369**, 3198 (2011).

<sup>11</sup>COMSOL MULTIPHYSICS 4.2a (2011), COMSOL Inc. (<http://www.comsol.com/>).

<sup>12</sup>K. N. Altmann, N. Gilman, J. Hayoz, R. F. Willis, and F. J. Himpsel, *Phys. Rev. Lett.* **87**, 137201 (2001).

<sup>13</sup>W. H. Butler, X.-G. Zhang, D. M. C. Nicholson, and J. M. MacLaren, *J. Magn. Magn. Mater.* **151**, 354 (1995).

<sup>14</sup>P. E. Mijnders, S. Sahrakorpi, M. Lindroos, and A. Bansil, *Phys. Rev. B* **65**, 075106 (2002).

<sup>15</sup>Y. Fukuma, L. Wang, H. Idzuchi, S. Takahashi, S. Maekawa, and Y. Otani, *Nat. Mater.* **10**, 527 (2011).

<sup>16</sup>G.-X. Miao, M. Müller, and J. S. Moodera, *Phys. Rev. Lett.* **102**, 076601 (2009).

<sup>17</sup>K. Senapati, M. G. Blamire, and Z. H. Barber, *Nat. Mater.* **10**, 849 (2011).